# Electrospinning recombinant spider silk fibroin-reinforced PLGA membranes – a biocompatible scaffold for would healing applications

| | |
|---|---|
| Journal: | *ACS Biomaterials Science & Engineering* |
| Manuscript ID | Draft |
| Manuscript Type: | Article |
| Date Submitted by the Author: | n/a |
| Complete List of Authors: | chen, yuanyuan; Technological University of the Shannon Midlands Midwest - Athlone Campus<br>Murphy, Emma; Technological University of the Shannon Midlands Midwest<br>Cao, Zhi ; Technological University of the Shannon Midlands Midwest - Athlone Campus<br>Buckley, Ciara; Technological University of the Shannon Midlands Midwest - Athlone Campus<br>Cortese, Yvonne; Technological University of the Shannon Midlands Midwest - Athlone Campus<br>Chee, Bor Shin; Technological University of the Shannon Midlands Midwest - Athlone Campus<br>Scheibel, Thomas; University of Bayreuth, Department of Biomaterials |
| | |

# Electrospinning recombinant spider silk fibroin-reinforced PLGA membranes – a biocompatible scaffold for would healing applications

Yuanyuan Chen[1*], Emma J. Murphy[1], Bor Shin Chee[1], Zhi Cao[1], Ciara Buckley[1], Yvonne Cortese[1], Thomas Scheibel[3]

[1] Polymer, Recycling, Industrial, Sustainability and Manufacturing (PRISM), Technological University of the Shannon: Midlands Midwest, Ireland

[2] University of Bayreuth, Department of Biomaterials, Prof.-Rüdiger-Bormann Str. 1, 95447 Bayreuth, Germany

[*] *Corresponding author Yuanyuan.Chen@tus.ie*

Keywords:

Polylactide-polyglycolide, recombinant spider silk fibroin, reinforcement, mechanical properties, electrospinning

**Abstract**

Polylactide-polyglycolide (PLGA) is one of the most attractive polymeric biomaterials used to fabricate medical devices for drug delivery and tissue engineering applications. Nevertheless, the utilisation of PLGA in load-bearing applications is restricted due to its inadequate mechanical properties. This study examines the potential of recombinant silk fibroin (eADF4), a readily producible biomaterial, as a reinforcing agent for PLGA. The PLGA/eADF4 composite membranes were developed using the process of electrospinning. The spinnability of the electrospinning solutions, as well as the physicochemical, mechanical, and thermal properties of the composite membranes, were characterized. The addition of eADF4 increased the viscosity of the electrospinning solutions and enhanced both the mechanical characteristics and thermal stability of the composites. This study demonstrates that PLGA membranes reinforced with recombinant spider silk fibroin are non-cytotoxic, significantly enhance cell migration and wound closure, and do not trigger an inflammatory response, making them ideal candidates for advanced wound healing applications.

## 1. Introduction

The skin, as the body's largest organ, plays a vital role in safeguarding against infections and preventing excessive water loss. When the skin is compromised by injury, burns, or disease, it activates repair mechanisms to restore its protective functions. However, in cases of severe damage, the skin may lose its natural ability to heal, resulting in chronic wounds, scarring, and loss of function. Wound healing is a complex physiological process, and chronic wounds pose significant challenges in healthcare, contributing to substantial patient distress and elevated mortality rates [1,2].

Managing wounds requires innovative and effective treatment strategies, with regenerative engineering playing a key role in this effort. This rapidly advancing field focuses on developing biomaterials and scaffolds that facilitate the repair and regeneration of damaged skin tissue. A critical challenge in skin tissue regenerative engineering is designing scaffolds that provide adequate mechanical support, closely mimicking the mechanical properties of natural skin to maintain structural integrity [3]. The scaffold must be strong enough to support regenerating tissue without collapsing, yet flexible enough to avoid stress-shielding, which could impede proper cell growth and integration with surrounding tissues [4]. Achieving this balance of mechanical strength and flexibility is essential for the successful regeneration of skin.

Polylactide-polyglycolide (PLGA) is a linear synthetic copolymer composed of lactic acid (LA) monomers and glycolic acid (GA) monomers at different ratios. With a tuneable biodegradability, PLGA has been currently mainly used as a delivery vehicle for drugs, proteins and various other macromolecules such as DNA, RNA and peptides [5]. PLGA also has good biocompatibility and is approved for clinical use in humans by the FDA, which makes PLGA an ideal candidate for tissue engineering applications. However, the poor mechanical properties of PLGA have limited its use in load-bearing tissue engineering applications, such as bone tissue engineering, and artery vascular tissue engineering [6,7,8]. To improve its mechanical properties, bioactive glass [9], cellulose nanocrystals [10], $TiO_2$ nanoparticles [11], hydroxyapatite microspheres [12], graphene oxide nanoparticles [13], etc. have been investigated as reinforcing materials for PLGA.

Natural spider silk fibres are increasingly recognized in medical fields for their excellent biodegradability, biocompatibility, and robust mechanical properties. Its applications span across various domains, including vascular implants [14], blood vessel sutures [15], and cardiac tissue engineering [16]. The mechanical strength of spider silk fibres is remarkable, with a strength of 1.1 GPa, rivalling that of high-tensile steel at 1.5 GPa and surpassing human bone strength by nearly sevenfold [9,10]. Additionally, its toughness exceeds many top-tier synthetic materials, including Kevlar® [17]. Therefore, spider silk fibres have been reported to be used as reinforcing materials. For instance, Bobylev and colleagues incorporated spider silk into cardiovascular patches, resulting in a significant enhancement of their mechanical properties, with a 1.8-fold increase in tensile force and a 1.45-fold increase in tensile strength [18]. However, these advancements face a significant challenge: the spider silk fibres used in these studies are sourced from various natural spiders, which are predominantly cannibalistic and difficult to farm collectively. This limitation makes the commercial mass production of natural spider silk fibre-reinforced polymer composites challenging.

Recombinant spider silk protein eADF4 is a genetically engineered spider silk protein produced in large quantities using *Escherichia coli* as a host[19]. Compared to natural spider silk fibre, recombinant spider silk proteins eADF4 offer several advantages, including 1) Controlled and Scalable Production. Unlike natural spider silk, which is challenging to harvest in large quantities due to the territorial and cannibalistic nature of spiders, eADF4 can be produced efficiently in microbial systems, ensuring a reliable and scalable supply for industrial and

biomedical applications. 2) Tailored Mechanical Properties. The genetic engineering of eADF4 allows for precise manipulation of its amino acid sequence, enabling the customization of mechanical properties such as tensile strength, elasticity, and degradation rates to suit specific needs, which is not possible with natural spider silk. 3) Consistent Quality. Recombinant production ensures a high level of purity and uniformity in eADF4, free from the variability found in natural silk fibres, which can be affected by environmental factors and spider species. This consistency is crucial for applications requiring precise material characteristics. 4) Good Compatibility. eADF4 retains the biocompatibility of natural spider silk, making it suitable for a range of biomedical applications, including tissue engineering and drug delivery [20,21].

This study explores the potential of eADF4 as a reinforcing agent to enhance the mechanical properties of PLGA membranes. It delves into a detailed examination of the electrospinnability, mechanical and thermal properties, as well as the morphology of the electrospun PLGA membranes reinforced with recombinant spider silk protein eADF4. The PLGA membranes were evaluated using an in vitro wound model with human keratinocytes to assess their potential for use in tissue engineering applications. This involved examining their impact on cell viability, wound closure ability, and potential irritancy, with IL-8 release measured following both direct and indirect exposure to the membranes.

## 2. Material and Methods

### *2.1 Materials*

PLGA was obtained from Ashland (Viatel™, Ireland) as a medical grade copolymer with a lactide and glycolide co-polymer ratio of 50:50 and a molecular weight of Mn 8,500 and Mw 19,100. Hexafluoroisopropanol (HFIP) was purchased from Abcr (Abcr GmbH, Germany). The recombinant spider silk fibroin eADF4(C16), which consists of 16 repeats of a C module (sequence: GSSAAAAAAAASGPGGYGPENQGPSGPGGYGPGGP) to mimic the repetitive core sequence of the European garden spider's (*Araneus diadematus*) dragline silk fibroin, was prepared as previously described [22,23].

### *2.2 Electrospinning solution preparation*

Firstly, the spinnability of the PLGA solution was determined by dissolving PLGA in HFIP at concentrations of 10, 25, and 50 wt%. The spinning solutions were characterized by dynamic viscosity and PLGA at 25% wt/v was chosen for further experiments. Secondly, 250 mg PLGA was dissolved in 0.5 ml HFIP and 0, 1, 5, 10, 20 wt% eADF4 prepared by dissolving 0, 5, 25, 50 and 100 mg eADF4 in 0.5 ml HFIP. Then, the 0.5 ml PLGA solution and 0.5 ml eADF4 solution were mixed to yield a 1 ml electrospinning solution. The composition of the electrospinning solutions is described in Table 1.

The dynamic viscosity of the spinning solutions was measured by using a TA instruments HR30 hybrid rheometer. Samples were analysed under shear rates of 1 to 1000 $s^{-1}$ to compare the viscosity and stress of samples. The axial force applied was constrained to 0.1 ± 0.01N.

*Table 1: Composition of PLGA/eADF4 electrospinning solutions using HFIP as the solvent*

| Sample | PLGA wt/v% | eADF4 wt/v% | PLGA: eADF4 ratio |
|---|---|---|---|
| PLGA | 25 | 0 | N/A |
| PLGA/eADF4-0.5 | 25 | 0.5 | 1:0.02 |
| PLGA/eADF4-2.5 | 25 | 2.5 | 1:0.1 |
| PLGA/eADF4-5 | 25 | 5 | 1:0.2 |
| PLGA/eADF4-10 | 25 | 10 | 1:0.4 |

*2.3 Membrane preparation*

The electrospinning process was performed in a custom-built device, with a chamber humidity of 26%, at an electrospinning solution flow rate of 0.42 ml/hour through a 21G needle (inner diameter 0.56 mm), which was positively charged at 16 kV. Fibres were deposited on a metal plate with a 10 kV negative charge. The distance between the needle and the plate remained at 100 mm. The electrospun membrane was collected after electrospinning for 2 hours.

*2.4 Morphology*

Scanning electron microscopy (SEM) was performed using a Mira XMU SEM (Tescan™, Czech Republic) in backscattered electron mode for surface analysis. The accelerating voltages utilized were 20 kV. Prior to analysis, test samples were placed on an aluminium stub, and the samples were sputtered with gold using Baltec SCD 005 for 110 s at 0.1 mbar vacuum before testing. TESCAN EssenceTM software was used to measure the fibre diameter and a number of 40-50 data was collected from each SEM image, a normality test was performed by plotting a histogram for a visual indication of normality. In a normal distribution, the histogram should appear bell-shaped.

*2.5 Fourier transfer infrared spectroscopy*

Attenuated total reflectance Fourier transform infrared spectroscopy (FTIR) was carried out on a PerkinElmer Spectrum One (USA) fitted with a universal ATR sampling accessory. All data was recorded at 21 °C in the spectral range of 650 - 4000 $cm^{-1}$ against the air as background, utilising a 4 scan per sample cycle at a resolution of 0.5 $cm^{-1}$ and a fixed universal compression force of 70 - 80 N. Subsequent analysis was carried out using Spectrum software.

*2.6 Mechanical testing*

The mechanical properties of the samples were characterised by tensile tests. Tensile testing was carried out on a Lloyd TA1 tensometer (Ametek Ltd., West Sussex, UK) using a 20 N load cell on ASTM standard test specimens at a strain rate of 5 mm/min. Data was recorded using Nexygen™ software. The tensile tests were carried out in adherence to ASTM D 882. Five replicates were analysed per group, and prior to testing the thickness of each sample was measured. The percentage strain at maximum stress, maximum stress, and Young's Modulus of each sample were recorded.

*2.7 Differential scanning calorimetry*

Differential scanning calorimetry (DSC) was carried out using a PerkinElmer DSC 4000 (USA) with a nitrogen flow rate of 20 ml/min to prevent oxidation. Calibration of the instrument was performed using indium as standard. Test specimens weighed between 8 and 12 mg were measured on a Sartorius scale (MC 210 P, Germany). Samples were crimped in non-perforated aluminium pans, with an empty crimped aluminium pan used as a reference. The samples were heated from 10 °C to 90 °C at a rate of 10 °C/min. The glass transition temperature of PLGA and PLGA/eADF4 composite was recorded.

*2.8 Thermogravimetric analysis*

The thermal stability of samples was tested using a PerkinElmer Pyris TGA 1 (USA), coupled with a PerkinElmer Thermal Analysis controller TAC7/DX under a nitrogen atmosphere. The tests for PLGA and PLGA/eADF4 composite were run from 30 °C to 650 °C, all experiments were performed at a heating rate of 10 °C/min.

*2.9 Culturing of HaCaT cells*

HaCaT cells were grown in high glucose Dulbecco's modified Eagle's medium (DMEM) (Thermofisher Scientific), with the addition of 10% fetal bovine serum (FBS) (ThermoFisher Scientific), 1% penicillin/streptomycin (ThermoFisher Scientific), and 2 mM L-glutamine (ThermoFisher Scientific). The cells were maintained in a humidified atmosphere at 37 °C with 5% CO2 in a CO2 incubator. They were cultured in T75 cm² flasks, and the growth medium was refreshed every 48 to 72 hours. Cell confluence was assesed using light microscopy. HaCaT cells were sub-cultured by trypsinization at 70% to 80% confluency. For viability assays, HaCaT cells were seeded at a density of $2.5\times10^4$ cells per well in flat-bottom 96-well plates (Sarstedt). For wound healing assays, HaCaT cells were seeded $4\times10^5$ per well in flat-bottom 24-well plates (Sarstedt).

*2.10 Viability Assay*

Viability was assessed after 72 hours using the Methyl Thiazolyl Tetrazolium (MTT) assay to evaluate the cytotoxicity of PLGA and PLGA/eADF4 composite membranes (PLGA/eADF4-0.5; PLGA/eADF4-2.5; PLGA/eADF4-5; PLGA/eADF4-10) in the context of wound healing. Experimental groups included these membrane concentrations along with controls: a non-viable cell control (Triton X-100 treated), an untreated control, and a dimethyl sulfoxide (DMSO) blank. All groups were tested in six replicates.
PLGA and PLGA/eADF4 composite membranes were prepared with a surface area of 30 cm², following ASTM standard [24], and sterilized with 70% isopropyl alcohol (IPA) and phosphate-buffered saline (PBS). Two exposure methods were tested: direct and indirect. For direct exposure, cells were incubated in 96-well plates with membranes cut to 6 mm to fit each well. For indirect exposure, 6 mm membranes were incubated in 100 µL of media for 72 hours, after which the membrane was removed, and the conditioned media was applied to the cells.

*2.11 In Vitro Wound Healing Scratch Assay*

HaCaT cells were seeded at a concentration of of $4\times10^5$ cells per well in 24-well plates and incubated at 37°C in a humidified atmosphere with 5% CO2. Once a monolayer was established, as confirmed by microscopic observation, scratches were made across the diameter of the wells using a sterile 1000 µL pipette tip. The culture medium was then aspirated, and each well was washed four times with serum- and additive-free DMEM. Subsequently, the cells were incubated with composite membranes (12 mm in diameter). Images of the wells were captured immediately after the scratches were made and at 16-hour intervals over a total period of 64 hours, using an EVOS cell imaging system. Throughout the experiment, the plates were maintained in a humidified environment with 5% CO2 at 37°C. Wound surface area was measured using EVOS imaging software, and the closure rate (µm²/h) was calculated.

*2.12 Assessment of Cell Migration*

To assess the potential migration of cells onto the membrane, CellTracker™ Green CMFDA (5-chloromethylfluorescein diacetate) (Thermo Fisher Scientific, catalog number: C7025) was used. A stock solution (50 µg of the probe in 20 µl of DMSO) was diluted in 2 ml of PBS, and the cells were incubated in this medium for 30 minutes at 37°C. Following this incubation, the cells were transferred into complete DMEM for an additional 30 minutes at 37°C.

*2.13 IL-8 ELISA*

To assess potential irritancy or inflammatory response, cell supernatants were collected after 72 hours of direct exposure to the membranes. IL-8 cytokine levels were quantified using specific sandwich enzyme-linked immunosorbent assays (ELISA) (Invitrogen), following the manufacturer's instructions.

*2.14 Statistical analysis*

Statistical analysis was performed using one-way analysis of variance (ANOVA) with a Tukey Post hoc test to determine differences. Differences were considered significant when $p \leq 0.05$. The software used to perform statistical analysis was SPSS (IBM Version 22) for Windows. All data collected in this study were expressed as mean ± standard deviation. A sample size of 5 was used for all experiments.

## 3. Results and Discussion

*3.1 Spinnability of the electrospinning solution*

The spinnability of a solution in electrospinning, which refers to its ability to be drawn into fine fibres, is significantly influenced by the polymer concentration. PLGA 10 wt% displayed strings of beads, while PLGA 25 wt% and PLGA 50 wt% demonstrated uniform fibres. This is related to polymer chain entanglements. At the core of electrospinning is the need for polymer chains to be sufficiently entangled. A higher polymer concentration typically increases the density of these entanglements. These entanglements are crucial because they provide the necessary cohesive force to draw the solution into a continuous fibre as it is ejected from the spinneret. This has been supported by other studies. Tiwari & Venkatraman dissolved PLGA in DMF/chloroform and reported a concentration range between 4 and 12% for producing uniform beadless fibres [25]. Zhou et al. dissolved poly(D, L-lactic acid) (PDLLA) in acetone and reported that uniformed beadless fibres were formed when PDLLA/acetone concentration (wt/v) reached 7.5% [26]. In addition, polymer concentration directly affects the viscosity of the solution. A higher concentration usually leads to higher viscosity. The right viscosity is essential for forming a stable jet and preventing bead formation. If the viscosity is too low, the solution may not form continuous fibres and instead break into droplets. If the viscosity is too high, the solution may be too thick to be effectively electrospun. The dynamic viscosity measures revealed that an increase in PLGA concentration increased the viscosity of the PLGA solution. PLGA 50 wt% outperformed PLGA 10 wt% and PLGA 25 wt% by approximately 6 and 3 folds, respectively ($p < 0.05$, Figure 1 a). However, high viscosity would result in difficulty in electrospinning, therefore PLGA 25wt% with medium viscosity and correspondingly resulting uniform fibres were chosen for further electrospinning solution formulations. Furthermore, PLGA 50 wt% exhibited a significant shear-thinning behaviour, compared to PLGA 10 wt% and PLGA 25 wt%, this can be explained that at 50% loading, the eADF4 in PLGA matrix is high enough to form a structure and entangled network through intermolecular hydrogen bonds, which responded to applied shear stress and became align and disentangled under shear stress, causing a decrease in viscosity [27].

PLGA 25 wt% was mixed with eADF4 at concentrations of 0.5, 2.5, 5, and 10 wt%. Dynamic viscosity measurements revealed that as the eADF4 concentrations increased, the viscosity of the PLGA/eADF4 dopes significantly increased accordingly ($p < 0.05$, Figure 1 b). In addition, all the PLGA/eADF4 dopes displayed decreased viscosity with increasing shear stress, which indicated the shear-thinning pseudoplastic behaviour of the dopes. Several studies using silk fibroin dopes reported similar shear-shinning properties [14,15]. It can be explained that the entangled PLGA polymer chains and eADF4 molecules were loosely packed in suspension; at low shear rates, the randomly and loosely packed structures exhibited high viscosity; as the stress increased, the structure became more oriented and stretched, exhibiting a reduced viscosity.

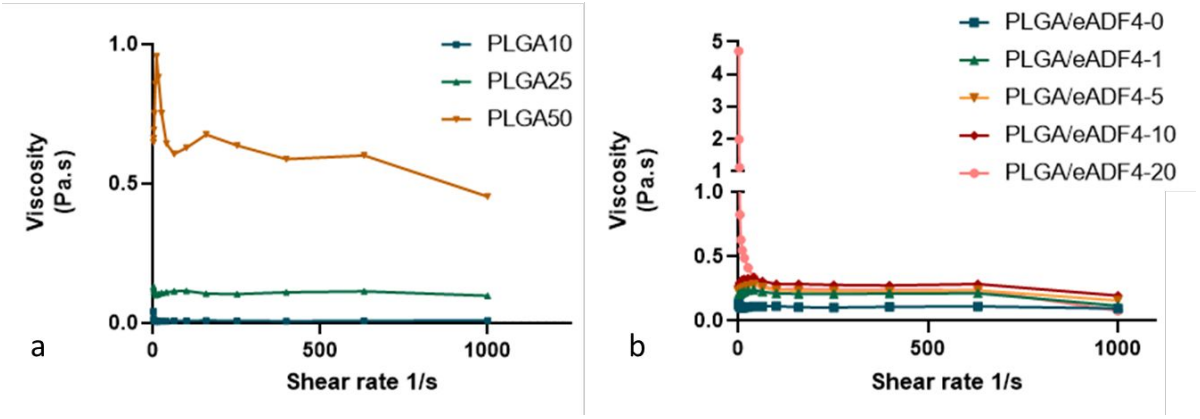


*Figure 1: a) Dynamic viscosity measurements of PLGA solutions p<0.05, b) Dynamic viscosity measurements of PLGA/eADF4 mixture solutions. p<0.05, sample size n=5.*

### *3.2 Physico-chemical properties of the electrospun PLGA/eADF4 membranes*

IR spectra of PLGA and PLGA/eADF4 membranes exhibited molecular vibrations of functional groups as illustrated in Figure 2. The characteristic peaks of PLGA include an intense peak at 1750 $cm^{-1}$, which is associated with the stretching vibration of the carbonyl C=O group, and the bands at 1300 $cm^{-1}$ and 1100 $cm^{-1}$, which were attributed to C-O and C-O-C groups [28]. The amide I band of eADF4 at 1700-1600 $cm^{-1}$ is primarily due to the C=O stretching vibration, amide Ⅱ band at 1600-1480 $cm^{-1}$ is related to the coupling of the N-H in-plane bending and C-N stretching, amide Ⅲ band at 1350-1190 $cm^{-1}$ is associated to C-N stretching coupled to the in-plane N-H bending, and amino acid side chains are corresponding to the absorption bands at 1480-1350 $cm^{-1}$ and 1190-700 $cm^{-1}$ [26].

Both characteristic peaks of PLGA and eADF4 can be observed in the PLGA/eADF4 composites. The peaks at 1654 $cm^{-1}$ and 1546 $cm^{-1}$ of eADF4 in Figure 2 are based on the characteristic structure of eADF4, and the intensity of these characteristic peaks increased as eADF4 concentration increased, which confirmed the addition of eADF4 within the composites. The carbonyl C=O group and C-O-C group of PLGA shifted from 1750 and 1085 $cm^{-1}$ to 1755 and 1091 $cm^{-1}$ for PLGA/eADF4-10 respectively. These shifts indicated the chemical interactions between PLGA and eADF4. The amide groups in eADF4 contain N-H bonds that can act as hydrogen bond donors, while the carbonyl oxygen in the ester groups of PLGA can act as a hydrogen bond acceptor. When these two components are blended, the hydrogen from the amide N-H group can form a hydrogen bond with the oxygen of the C=O group in PLGA. This hydrogen bonding interaction stabilizes the carbonyl group, slightly lowering the electron density around the carbonyl carbon and oxygen. As a result, the energy required for the C=O stretching vibration increases, causing a slight shift to a higher wavenumber (from 1750 $cm^{-1}$ to 1755 $cm^{-1}$). The C-O-C group in the ester linkage is also susceptible to hydrogen bonding, though it primarily contributes to dipole-dipole interactions due to its polar nature. The oxygen atoms in the C-O-C group can engage in hydrogen bonding with the N-H groups in eADF4, or they can participate in dipole-dipole interactions with the nearby amide groups of eADF4. These interactions can similarly affect the electronic environment, making the C-O-C bond slightly more rigid or stabilized, leading to a shift to a higher wavenumber as observed [29, 30].

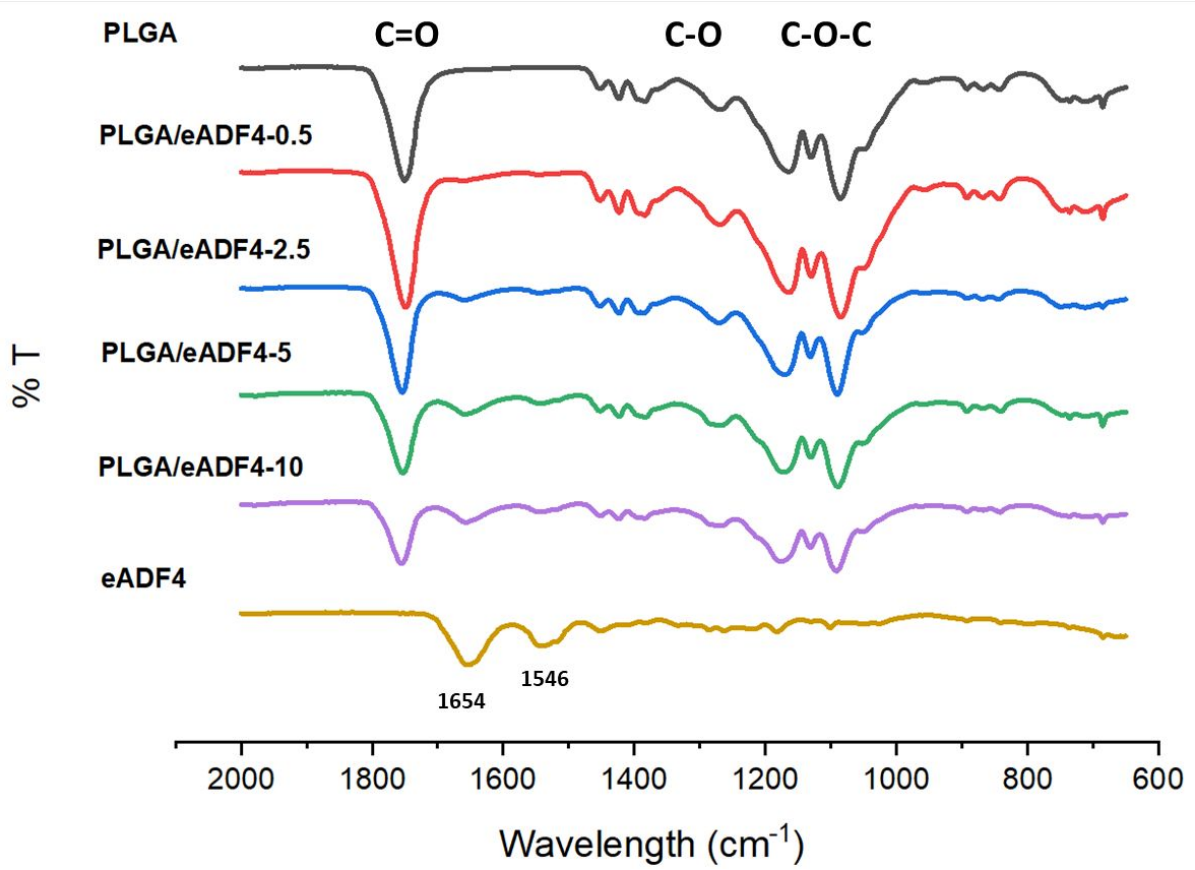


*Figure 2: FTIR spectra of PLGA, eADF4, and PLGA/eADF4 composite membranes. The PLGA/eADF4 composite membranes exhibited the characteristic peaks of both PLGA (1750 $cm^{-1}$ for the C=O group) and eADF4 (1700-1600 $cm^{-1}$ for the amide group). The intensity of the characteristic groups of eADF4 increased as the content of eADF4 increased.*

The morphology of PLGA and PLGA/eADF4 composites was analysed using SEM, as depicted in Figure 3. There is a clear trend of increasing fibre diameter with the increasing content of eADF4 in the composite. Fibre diameters of PLGA, PLGA/eADF4-0.5, PLGA/eADF4-2.5, PLGA/eADF4-5, and PLGA/eADF4-10 were measured to be 0.35 ± 0.099 µm, 0.33 ± 0.1 µm, 0.55 ± 0.21 µm, 1.04 ± 0.64 µm, and 2.18 ± 1.48 µm respectively. There was no significant difference between PLGA and PLGA/eADF4-0.5 (p=1), and PLGA and PLGA/eADF4-2.5 (p=0.812). As the eADF4 concentration was increased, the fibre diameter was increased, and there was a significant difference between PLGA and PLGA/eADF4-5 (p=0.007), PLGA and PLGA/eADF4-10 (P<0.001). The explanation could be that eADF4, being a protein-based polymer, increased the viscosity of the PLGA solution when added. An increase in the viscosity of the polymer solution led to a corresponding increase in resistance to flow, resulting in the production of thicker fibres. Furthermore, the incorporation of eADF4 into the solution leads to an augmentation of polymer chain entanglements, hence facilitating the creation of uninterrupted fibres during the electrospinning process. Similar results were reported by Boncu et al., they dissolved PLGA in HFIP and observed that an increase in polymer concentration led to an increase in the viscosity of the solution, resulting in the formation of fibres with larger diameters [31]. Furthermore, Meng et al. observed a similar relationship between polymer content and fibre diameter. They electrospun PLGA/chitosan solutions and reported that the increase in chitosan content increased the viscosity of the solution and resulted in fibre with a thicker diameter [32]. The findings of this study are consistent with the existing literature.

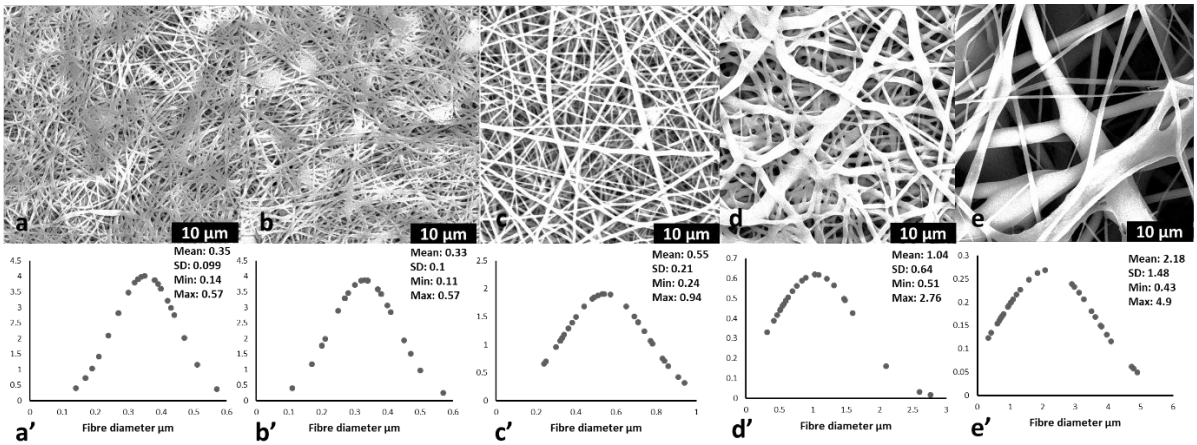


*Figure 3: SEM images of PLGA and PLGA/eADF4 membranes, and fibre diameters were measured. a and a') PLGA 0.35 ± 0.099 µm, b and b') PLGA/eADF4-0.5 0.33 ± 0.1 µm, c and c') PLGA/eADF4-2.5 0.55 ± 0.21 µm, d and d') PLGA/eADF4-5 1.04 ± 0.64 µm, e and e') PLGA/eADF4-10 2.18 ± 1.48 µm. There was no significant difference between PLGA and PLGA/eADF4-0.5 (p=1), PLGA and PLGA/eADF4-2.5 (p=0.812), as eADF4 concentration was increased further, the fibre diameter was increased, there was a significant difference between PLGA and PLGA/eADF4-5 (p=0.007), PLGA and PLGA/eADF4-10 (P<0.001).*

### *3.3 Mechanical properties*

The tensile testing results of PLGA/eADF4 membranes are listed in Table 1. There is a clear trend of increasing tensile strength and Young's modulus, along with decreasing ductility (strain at break), as the content of eADF4 in the composite increases. The maximum tensile stress exhibited a significant increase, rising from 1.27 ± 0.8 MPa for PLGA to 3.73 ± 0.6 MPa for PLGA/eADF4-2.5 ($p < 0.005$). The Young's modulus also exhibited a significant increase from 28.42 ± 4.4 MPa for PLGA to 44.21 ± 6.7 MPa for PLGA/eADF4-0.5, 86.7 ± 13.4 MPa for PLGA/eADF4-2.5, 71.02 ± 5.7 MPa for PLGA/eADF4-5, 80.52 ± 13.5 MPa for PLGA/eADF4-10 ($p < 0.01$ for all comparison). However, the strain at break was decreased from 14.24 ± 0.2% for PLGA to 10 ± 0.1% for PLGA/eADF4-0.5 ($p = 0.043$), 4.1 ± 0.4% for PLGA/eADF4-2.5 ($p = 0.004$), 2.2 ± 0.02% for PLGA/eADF4-5 ($p = 0.011$), 1.1 ± 0.01% for PLGA/eADF4-10 ($p = 0.01$).

*Table 1: Tensile testing results of PLGA and PLGA/eADF4 electrospun membranes (* indicated significance P<0.05).*

| Membrane | Maximum tensile stress MPa | Young's modulus MPa* | Strain at breaking%* |
|---|---|---|---|
| PLGA | 1.27±0.8* | 28.42±4.4 | 14.24±0.2 |
| PLGA/eADF4-0.5 | 1.51±0.4 | 44.21±6.7 | 10.0±0.1 |
| PLGA/eADF4-2.5 | 3.73±0.6* | 86.7±13.4 | 4.1±0.4 |
| PLGA/eADF4-5 | 1.65±0.2 | 71.02±5.7 | 2.2±0.02 |
| PLGA/eADF4-10 | 0.86±0.2 | 80.52±13.5 | 1.1±0.01 |

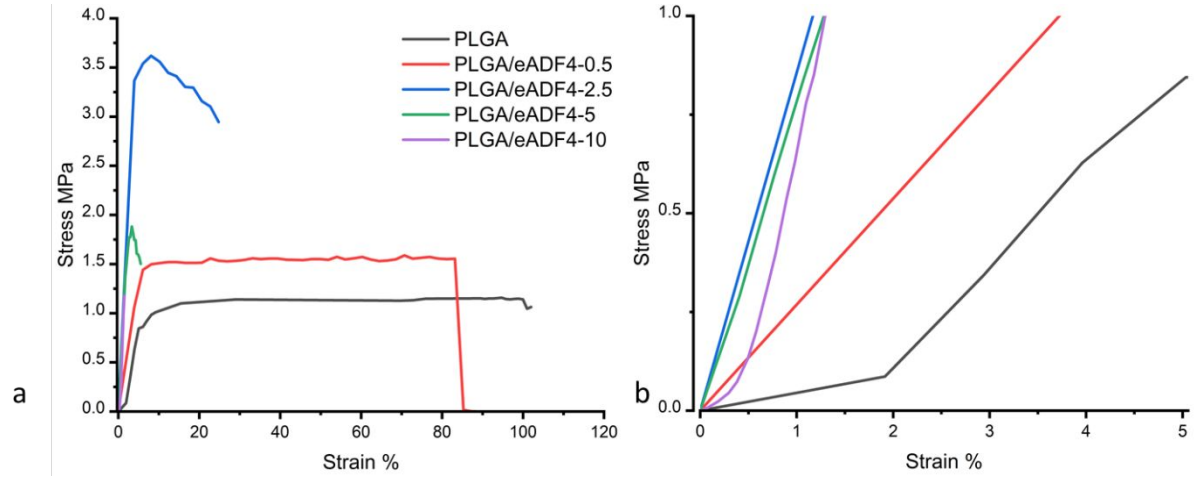


*Figure 4: Stress-strain curves of PLGA and PLGA/eADF4 electrospun membranes. a) The full scale of the stress-strain curves. b) The focused section of the stress-strain curves. The maximum tensile stress was significantly increased from 1.27 ± 0.8 for PLGA to 3.73 ± 0.6 for PLGA/eADF4-2.5, Young's modulus was significantly increased from 28.42 ± 4.4 MPa for PLGA to 44.21 ± 6.7 MPa for PLGA/eADF4-0.5, 86.7 ± 13.4 MPa for PLGA/eADF4-2.5, 71.02 ± 5.7 MPa for PLGA/eADF4-5, 80.52 ± 13.5 MPa for PLGA/eADF4-10 ($P<0.05$), sample size n=5.*

The observed increase in stress and Young's modulus, along with the decrease in ductility in the PLGA/eADF4 composites, can be explained by several key mechanisms related to the material properties and interactions between PLGA and eADF4: 1) Reinforcement effect of eADF4. eADF4, a protein with a highly ordered β-sheet secondary structure, acts as a reinforcing agent within the PLGA matrix. The crystalline regions of eADF4 contribute to the rigidity and stiffness of the composite material, which is evidenced by the increased maximum tensile stress and Young's modulus observed in the PLGA/eADF4-2.5 sample. The presence of eADF4 enhances the load-bearing capacity of the composite, leading to an overall increase in the mechanical strength of the material. The highest tensile stress was recorded at 3.73 ± 0.6 MPa for the PLGA/eADF4-2.5 composite, which represents a significant improvement over the pure PLGA matrix. 2) Load bearing capacity. The addition of eADF4 enhances the composite's ability to distribute applied stress more evenly across the material. This is particularly true for the tensile stress, where the eADF4 protein structures are capable of bearing a significant portion of the applied load, reducing the strain on the PLGA matrix and thereby increasing the material's tensile strength and Young's modulus. 3) Interfacial bonding and load shifting. The interaction between PLGA and eADF4 is crucial for effective stress transfer within the composite. The observed improvements in tensile stress and Young's modulus suggest strong interfacial bonding between the PLGA and eADF4 components. This bonding facilitates the efficient transfer of stress from the softer PLGA matrix to the stiffer eADF4 structures, thereby enhancing the overall mechanical performance of the composite. As the eADF4 content increases, the ability of the composite to transfer load from the PLGA matrix to the eADF4 structures improves, contributing to the increased stiffness and strength observed in the composite. 4) Restriction of polymer chain mobility. The addition of eADF4 restricts the mobility of PLGA polymer chains. The rigid eADF4 structures limit the ability of the PLGA chains to move and deform, leading to a decrease in the material's ductility. This is evidenced by the significant reduction in elongation at maximum stress, which dropped from 14.24 ± 0.2% in pure PLGA to just 1.1 ± 0.01% in the PLGA/eADF4-10 composite [33]. This change in mechanical properties was also reported by Venkatesan et al. They utilized silk fibroin to reinforce polycinylalcohol and polyvinyl pyrrolidone composites. The tensile strength and Young's modulus increased, and the elongation at break reduced significantly when the silk fibroin was added. They gave a similar explanation in stress transfer mechanism

and polymer chain mobility restriction [34]. Similarly, Gao et al. reported increased Elastic modulus and reduced elongation with PLLA/silk fibroin composite [35]. Zhao et al. found that incorporating 30% spider silk fibroin into PDLLA significantly enhanced its tensile strength from 1.8 MPa to 3.7 MPa [26]. The findings of this study are consistent with the literature.

It is worth noting that the tensile strength of the composite material increased to a maximum of 3.73 ± 0.6 MPa with the addition of 2.5% eADF4, after which it decreased with further increases in the eADF4 content. This trend suggests an optimal concentration of eADF4 where the reinforcing effects are maximized. Beyond this optimal concentration, the tensile strength decreases, which can be attributed to the aggregation of eADF4 fibres and possible phase separation, leading to poor dispersion within the PLGA matrix. This phenomenon has been observed and reported in several studies. Noishiki et al. studied silk fibroin and microcrystalline cellulose composites and reported that the Young's modulus of the composites showed a linear dependence on the increasing cellulose content, while the tensile strength showed a maximum at an optimal concentration of cellulose[21].

*3.4 Thermal stability*

The thermal stability of the PLGA/eADF4 composite membranes was studied since the thermal stability study not only provides information for potential further thermal processes but also provides intrinsic properties of the material. The used PLGA is a copolymer with a lactide and glycolide co-polymer ratio of 50:50, therefore the glass transition temperature ($T_g$) is around 40 – 60 ˚C [36]. From the DSC thermograms of PLGA and PLGA/eADF4 composites in Figure 5a, it can be seen that for PLGA/eADF4 composites with lower concentrations of eADF4 (0.5%, 2.5%, and 5%), the DSC curves show no significant shift in the $T_g$. This suggests that at these lower concentrations, the eADF4 does not substantially interact with the PLGA matrix to alter the $T_g$. The polymer matrix likely maintains its original chain dynamics, with eADF4 acting as a relatively passive filler. The DSC curve for PLGA/eADF4-10 shows a significant shift in $T_g$ to 56°C. This substantial shift suggests that at this higher concentration, eADF4 has a more pronounced interaction with the PLGA matrix. This is because a high concentration of eADF4 hindered the PLGA polymer chain mobility, thus requiring more energy for the PLGA chain to move. A similar increase in $T_g$ with the addition of silk fibroin was reported in a study of silk fibroin-reinforced polycinylalcohol and polyvinyl pyrrolidone composites [33], and a study in PLLA/silk fibroin composites [35]. PLGA is an amorphous material that doesn't show crystallization and doesn't have a melting temperature. However, silk can affect the crystallization and melting behaviour of semicrystalline polymers. A study in spider silk reinforced polycaprolactone (PCL) composites reported that the addition of 15 - 55 wt% spider silks increased the crystallization and melting temperatures of PCL, due to the nucleation effect of the spider silks [37]. In addition, the intensity of the $T_g$ peak was reduced as eADF4 added, this maybe explained by 1) Dilution effect. As eADF4 is added, the relative proportion of PLGA in the composite decreases. Since the $T_g$ peak corresponds primarily to the PLGA matrix, its intensity might reduce simply because there is less PLGA to contribute to the thermal signal. This dilution effect on the $T_g$ of polymer blends has been reported widely [38, 39, 40]. 2) Phase separation. When phase separation occurs at higher concentrations of eADF4, there may be regions within the material where PLGA is less affected by thermal transitions, reducing the overall intensity of the observed $T_g$. Phase-separated domains of eADF4 may not contribute to the $T_g$ in the same way as the more homogeneous PLGA matrix. The effect of phase separation on $T_g$ has been also widely reported [41, 42, 43].

TGA curves of PLGA and PLGA/eADF4 composites in Figure 5b exhibited two decomposition steps. The first decomposition step at 80 - 150 ˚C was due to the loss of water from the samples, and the second decomposition step at 290 - 500 ˚C was related to the polymer

structure degradation and breakdown of C-C bonds in the polymer backbone. It is revealed that a small amount of eADF4 at 0.5wt% didn't affect the onset degradation temperature of PLGA significantly, but as the eADF4 content increased, onset degradation temperature was increased, from 294˚C for PLGA to 325˚C, 324˚C, and 332˚C for PLGA/eADF4-2.5, PLGA/eADF4-5, PLGA/eADF4-10, respectively. The improved thermal stability of the PLGA/eADF4 composites is attributed to the high thermal stability of silk, which interacted with the PLGA polymer matrix and acted as a barrier for better heat insulation. Similarly, Gao et al. reported that the addition of 0.02 wt% silk fibroin in PLLA composite increased the initial thermal decomposition temperature of PLLA from 263 ˚C to 302 ˚C, and they attributed this effect to a substantial rise in the elastic modulus [35]. Sheik and Nagaraja reported that the addition of silk fibroin (3 - 15 wt%) significantly improved the thermal stability of the polycinylalcohol and polyvinyl pyrrolidone composites, and they explained with the high melting temperature of silk [33]. However, opposing results were reported in a study of silk fibroin-reinforced polyurethane composites, and the authors explained it by the phase separation with very high silk fibre contents (25, 50, 75, 90 wt%) in the composites [34]. The compatibility of composites is crucial, if the composite components are not compatible with each other, the properties of the composites would be deteriorated.

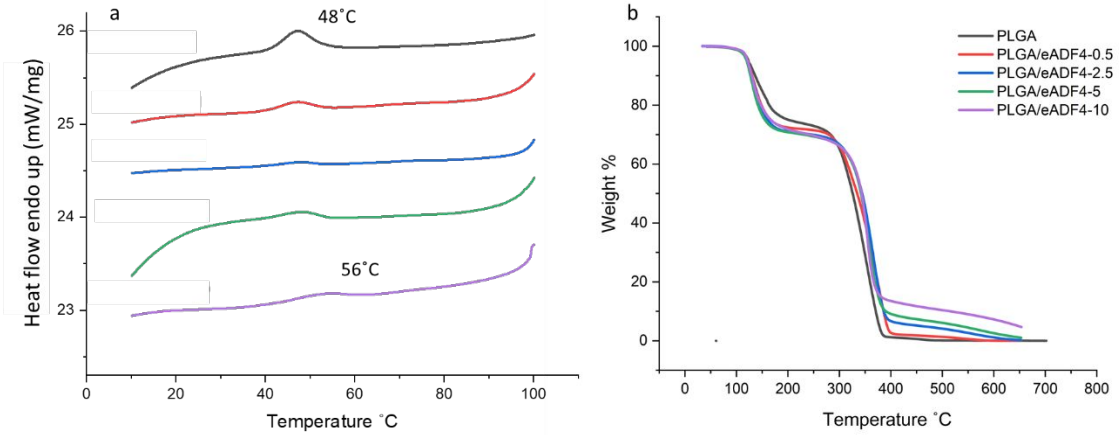


*Figure 5: a) DSC curves and b) TGA curves of PLGA and PLGA/eADF4 composites. The $T_g$ of PLGA increased from 48 ˚C to 56 ˚C for PLGA/eADF4-10, and the onset degradation temperature was increased from 294˚C for PLGA to 325˚C, 324˚C, and 332˚C for PLGA/eADF4-2.5, PLGA/eADF4-5, PLGA/eADF4-10, respectively. The incorporation of eADF4 improved the thermal stability of the PLGA/eADF4 composite membranes, sample size n=5.*

### *3.5 Cell culture*

HaCaT cells, a human keratinocyte cell line, were used in these assays to model the behaviour of skin cells during wound healing, as they closely mimic the regenerative and migratory properties of human epidermal cells. These assays were used to evaluate the biocompatibility, wound healing potential, and inflammatory response of PLGA and PLGA/eADF4 composite membranes, essential factors in developing effective materials for skin tissue regeneration.

In Figure 6, the analysis of HaCaT cell viability under both direct and indirect exposure to composite membranes demonstrated that all tested PLGA/ADF composites maintained cell viability comparable to the control group and did not exhibit any significant cytotoxic effects. This suggests that the composite membranes are biocompatible and do not adversely affect cell viability.

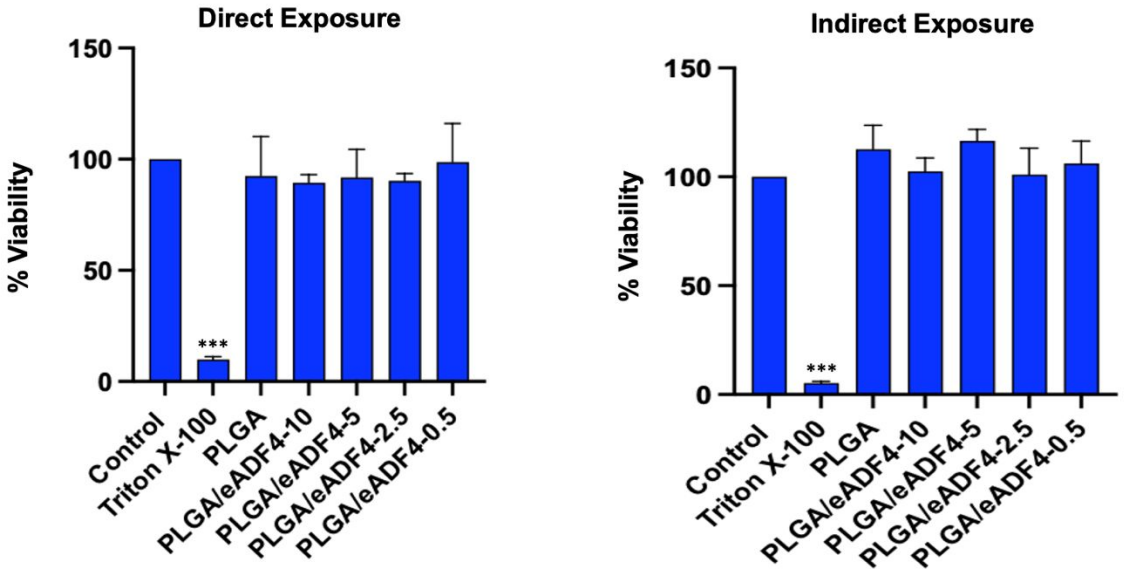


*Figure 6: Comparative analysis of HaCaT cell viability under direct and indirect exposure of composite membranes determined by MTT assay. Statistical significance compared to the control group was assessed using the Mann-Whitney U test, with significance indicated by asterisks (***$p < 0.001$). Triton X-100 was the only treatment that demonstrated a statistically significant reduction in viability in both direct and indirect exposure conditions, sample size n=5.*

The results depicted in Figure 7 from the wound healing assay demonstrate the migratory behaviour of HaCaT cells in response to various composite membranes. The initial scratch, with a width of 1000 µm, acts as a baseline to measure wound closure after 68 hours. The PLGA membrane (Panel C) demonstrated the most significant reduction in scratch width, down to 50 µm, suggesting that this composite significantly enhances cell migration. In contrast, the control sample (Panel B) showed a moderate reduction in scratch width to 350 µm, while the PLGA/eADF4-10 membrane (Panel D) resulted in a relatively larger scratch width of 400 µm, indicating slower cell migration compared to the control and PLGA. The PLGA/eADF4-5 (Panel E) and PLGA/eADF4-2.5 (Panel F) composites exhibited more effective migration than the control, with scratch widths of 300 µm and 250 µm, respectively, suggesting that these formulations also support wound healing, not as effective as PLGA alon. The PLGA/eADF4-0.5 membrane (Panel G) showed similar results to the control, with a scratch width of 350 µm, indicating no significant enhancement or reduction in cell migration. These findings demonstrate the potential of PLGA and PLGA/eADF4 (5 and 2.5) composites in promoting wound healing.

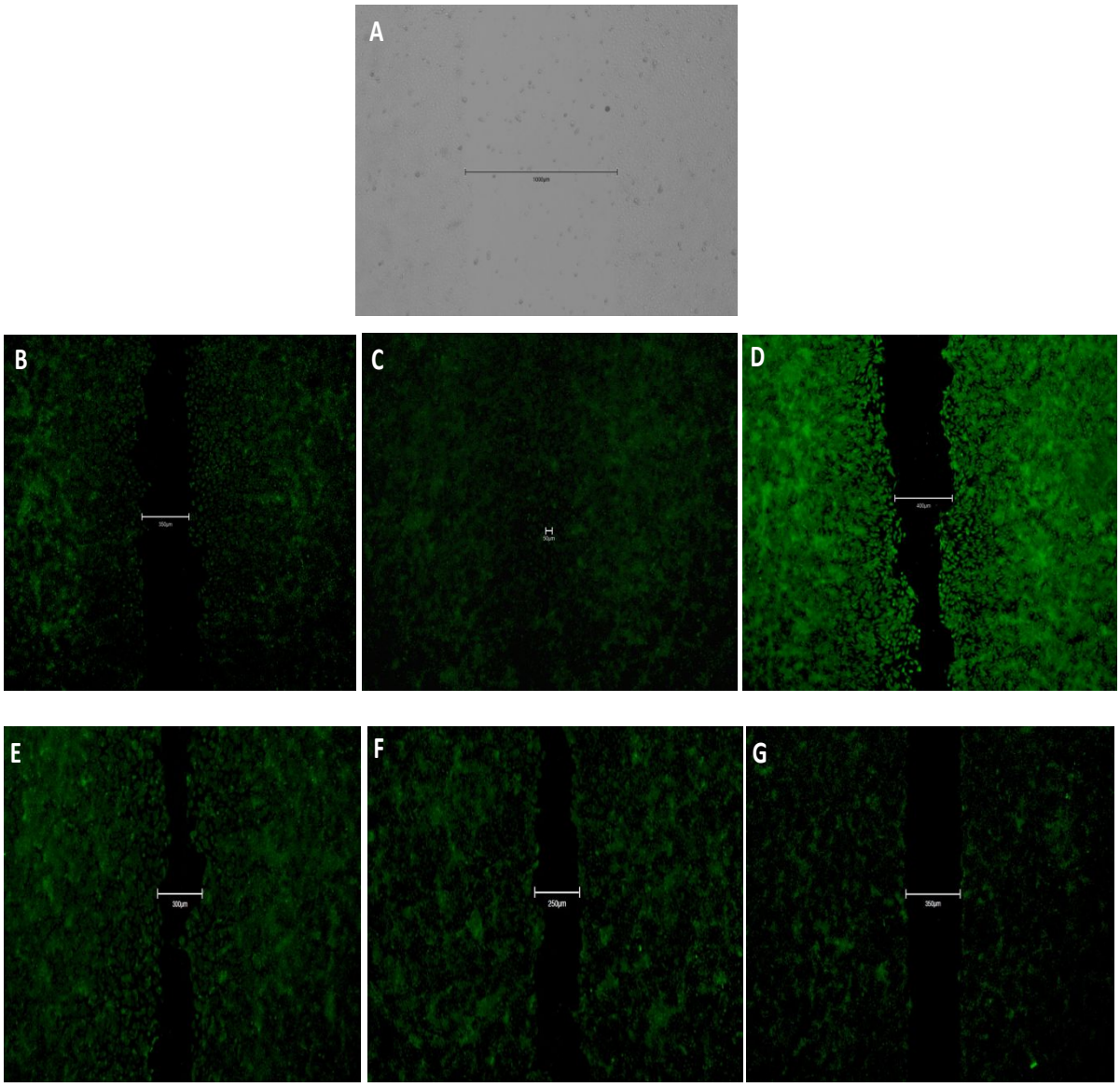


*Figure 7: Microscopic Analysis of Wound Healing Assay: Fluorescence Imaging of HaCaT Cells Stained with CellTracker™ Green CMFDA. Panel A shows the initial scratch at time 0, with a width of 1000 µm. Panels B through G display images taken 68 hours post-scratch, demonstrating the migration of HaCaT cells in the presence of the composite membranes. Panel B shows the control, where the scratch width was reduced to 350 µm. Panel C depicts the PLGA sample with a reduced scratch width of 50 µm. Panel D illustrates the PLGA/eADF4-10 membrane with a width of 400 µm, while Panel E shows PLGA/eADF4-5 with a width of 300 µm. In Panel F, the PLGA/eADF4-2.5 membrane resulted in a scratch width of 250 µm, andPanel G demonstrates the PLGA/eADF4-0.5 membrane with a width of 350 µm, sample size n=5.*

Figure 8 presents the scratch assay closure rates over four time points—16, 32, 48, and 64 hours statistically comparing the control group to samples treated with various composite membranes. The data indicate that at the earlier time points (16 and 32 hours), there were no statistically significant differences in closure rates among the different treatments, suggesting similar levels of cell migration across all groups during the initial phases of wound healing.

However, at the 48-hour time point, a significant increase in closure rate was observed for the PLGA-treated samples, with a highly significant difference (***$p < 0.001$) compared to the control. Suggesting like the date in figure 7 that PLGA enhances cell migration.

At 64 hours, a significant reduction in closure rate was noted for the PLGA/eADF4-0.5 treated samples (*$p < 0.05$), indicating that while this composite initially supports cell migration, its

effectiveness may decrease over time compared to the control. The other composites did not show significant differences in closure rates at this time point.

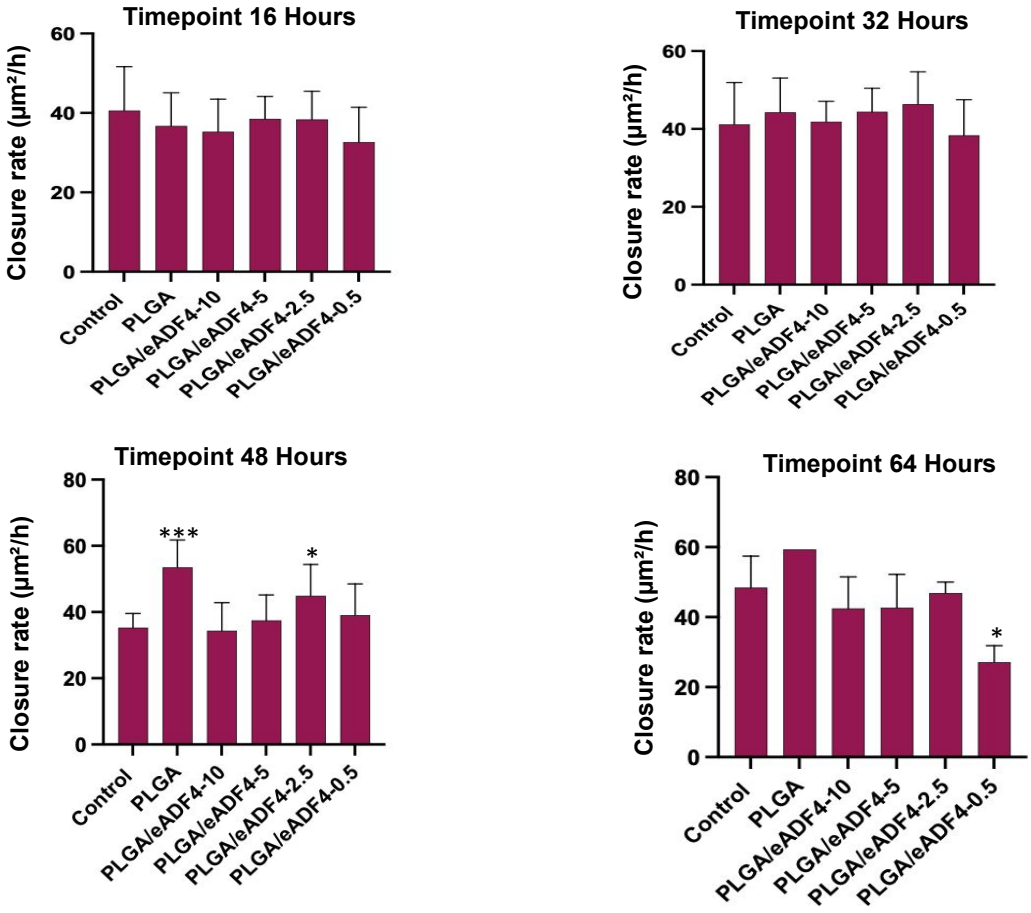


*Figure 8: Scratch Assay Closure Rates at 16, 32, 48, and 64 Hours. The graphs demonstrate the closure rates (µm²/h) of control and membrane-treated samples over different time points. Statistical significance was determined using t-tests, with *** indicating $p < 0.001$ and * indicating $p < 0.05$. At 48 hours, PLGA showed a highly significant difference (**). At 64 hours, PLGA/eADF4-0.5 showed a significant difference (*). No significant differences were observed for other samples at 16 and 32 hours, sample size n=5.*

Figure 9 shows the measurement of scratch diameter in HaCaT cells 68 hours post-scratch across various treatment groups, compared to the initial scratch width at T0. Results indicate that all treatment groups resulted in a statistically significant reduction in scratch width relative to the initial width (T0), confirming effective wound closure across all samples which is to be expected. The most significant reduction in scratch diameter was observed in the PLGA-treated group. This finding suggests that PLGA significantly promotes cell migration and wound closure more effectively than the other composite treatments. Other treatment groups, including those with PLGA/eADF4 composites, also showed significant reductions in scratch width.

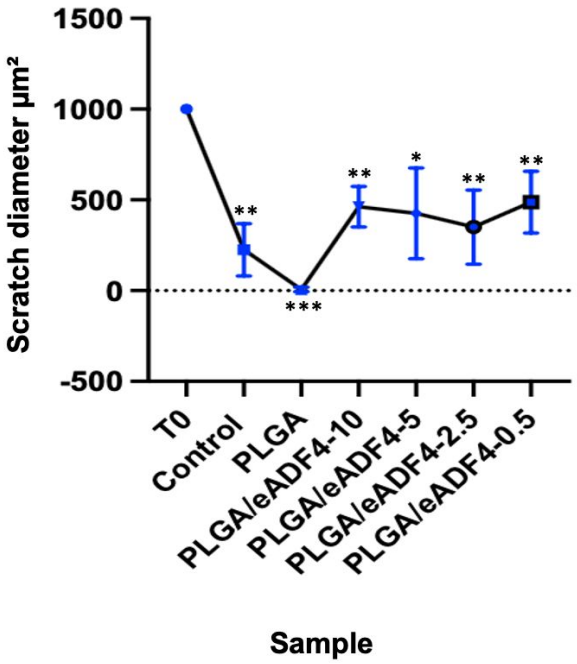


*Figure 9: Scratch Assay of HaCaT Cells: Measurement of Scratch Diameter at 68 Hours Post-Scratch Across Different Samples. A paired t-test was conducted to evaluate the significance of the difference between T0 and each treatment group. Statistically significant reductions in scratch width compared to T0 are indicated by the following symbols: *** for $p < 0.001$, ** for $p < 0.01$, and * for $p < 0.05$. All treatment groups showed significant reductions in scratch width compared to T0, highest significance observed in the PLGA group (***), sample size n=5.*

Figure 10 illustrates the secretion of IL-8 an inflammatory chemokine secreted from HaCaT cells, measured by ELISA, following both direct and indirect exposure to various composite membranes. The results show that SDS (0.01%), used as a positive control irritant, was the only treatment that significantly increased IL-8 levels compared to the control group This indicates an expected inflammatory response triggered by SDS.

In contrast, all the composite membrane samples, including PLGA and PLGA/eADF4 variants, did not induce a significant increase in IL-8 secretion, maintaining levels comparable to the control group. This suggests that these materials do not provoke an inflammatory response in HaCaT cells, highlighting their potential biocompatibility and suitability for applications where it is important not initiate further inflammation particularly in wound healing.

These findings demonstrate that PLGA and certain PLGA/eADF4 composites are non-cytotoxic, effectively promote cell migration and wound closure, and do not induce an inflammatory response, making them promising candidates for enhancing wound healing in regenerative applications.

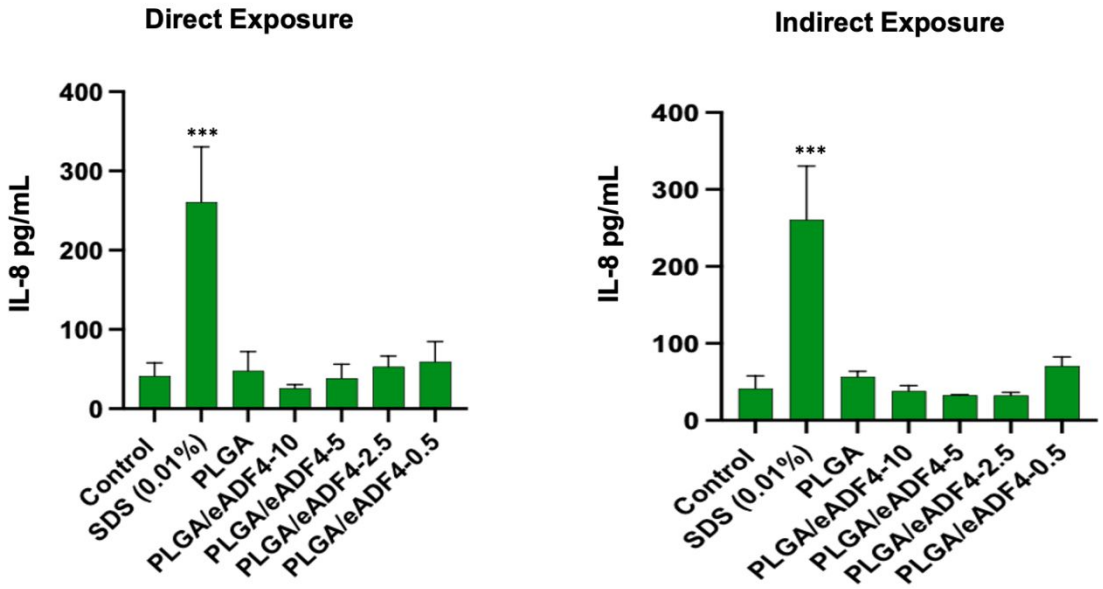


*Figure 10 : IL-8 Secretion in HaCaT cells determined by ELISA following direct and dndirect exposure to composite membranes. Statistical significance compared to the control group was assessed using the Mann-Whitney U test, with significance indicated by asterisks (***p < 0.001). SDS (0.01%) a positive control irrirant was the only treatment that demonstrated a statistically significant increase in IL-8 in HaCaT cells compared to controls, sample size n=5.*

Over all, the results indicate that PLGA and PLGA/eADF4 composites are promising candidates for enhancing wound healing in regenerative applications. The biocompatibility, promotion of cell migration, and absence of inflammatory responses underscore their potential in developing advanced wound care materials. The use of eADF4 is particularly intriguing due to its bioactive properties. As a recombinant spider silk protein, eADF4 offers unique benefits such as excellent mechanical strength, elasticity, and a favourable interaction with cells, all of which are crucial for the successful integration of scaffolds in tissue engineering [44,45,46]. The ability of eADF4 to modulate cell behaviour, possibly through its influence on cell adhesion, proliferation, and migration, suggests that it could play a key role in optimizing the wound healing process. Moreover, the absence of significant inflammatory responses in the presence of PLGA/eADF4 composites is particularly promising, as inflammation can hinder the healing process and lead to chronic wounds. This biocompatibility ensures that the materials will not exacerbate existing injuries or introduce new complications, making them suitable for long-term applications in wound care.

Future studies should focus on exploring the long-term effects of PLGA/eADF4 composites in vivo to better understand their performance in a more complex biological environment. Investigating the underlying mechanisms through which eADF4 modulates cell behaviour will be crucial in refining these materials. Such studies could reveal new insights into how eADF4 influences cellular responses, potentially leading to the development of even more effective regenerative scaffolds tailored to specific wound healing needs. Additionally, exploring the potential for customizing the mechanical and degradation properties of these composites could further enhance their effectiveness. By fine-tuning the balance between mechanical support and biodegradability, it may be possible to develop scaffolds that not only facilitate rapid wound closure but also seamlessly integrate with the body's natural healing processes, ultimately leading to improved outcomes for patients.

## 4. Conclusion

This study addressed the limitations of PLGA in load-bearing applications in tissue engineering due to its poor mechanical properties. PLGA and recombinant silk fibroin eADF4 at concentrations of 0.5, 2.5, 5, and 10 wt% were dissolved in HFIP, mixed with 25 wt% PLGA solution and electrospun. With the rise in eADF4 concentration, there was a notable increase in the viscosity of the PLGA/eADF4 solutions, resulting in the production of thicker fibres during the electrospinning process. By incorporating eADF4, the stiffness of PLGA was enhanced, but the ductility was reduced. Furthermore, integrating eADF4 improved the thermal stability of PLGA with elevated glass transition and onset degradation temperatures. The excellent cytocompatibility of the PLGA/eADF4 membranes indicates their promising potential for use in wound healing application.

## CRediT authorship contribution statement

Yuanyuan Chen: conceptualization, funding acquisition, methodology, investigation, project administration, visualization, and editing. Emma Murphy: performed cell culture study. Zhi Cao: performed TGA test. Yvonne Cortese: performed antimicrobial test and editing. Ciara Buckley: performed viscosity testing and editing. Thomas Scheibel: supervision, conceptualization, review & editing.

## Disclosures

The authors declare that there is no conflict of interest regarding the publication of this article, this manuscript has not been published elsewhere and it has not been submitted simultaneously for publication elsewhere. Thomas Scheibel is the co-founder and shareholder of AMsilk GmbH.

## Acknowledgements

This publication has been financially supported by the Irish Research Council New Foundation Programme. PLGA has been kindly donated by Ashland Specialties Ireland Limited.

## References

(1) Larouche, J.; Sheoran, S.; Maruyama, K.; Martino, M. M. Immune Regulation of Skin Wound Healing: Mechanisms and Novel Therapeutic Targets. *Adv. Wound Care* **2018**, *7* (7), 209–231. https://doi.org/10.1089/wound.2017.0761.

(2) Ellis, S.; Lin, E. J.; Tartar, D. Immunology of Wound Healing. *Curr. Dermatol. Rep.* **2018**, *7* (4), 350–358. https://doi.org/10.1007/s13671-018-0234-9.

(3) Albanna, Mohammad Z.; Holmes IV, J. H. *Skin Tissue Engineering and Regenerative Medicine*; Elsevier.

(4) Chen, J.; Fan, Y.; Dong, G.; Zhou, H.; Du, R.; Tang, X.; Ying, Y.; Li, J. Designing Biomimetic Scaffolds for Skin Tissue Engineering. *Biomaterials Science*. The Royal Society of Chemistry May 2, 2023, pp 3051–3076. https://doi.org/10.1039/d3bm00046j.

(5) Makadia, H. K.; Siegel, S. J. Poly Lactic-Co-Glycolic Acid (PLGA) as Biodegradable Controlled Drug Delivery Carrier. *Polym. 2011, Vol. 3, Pages 1377-1397* **2011**, *3* (3), 1377–1397. https://doi.org/10.3390/POLYM3031377.

(6) Gentile, P.; Chiono, V.; Carmagnola, I.; Hatton, P. V. An Overview of Poly(Lactic-Co-Glycolic) Acid (PLGA)-Based Biomaterials for Bone Tissue Engineering. *Int. J. Mol. Sci. 2014, Vol. 15, Pages 3640-3659* **2014**, *15* (3), 3640–3659. https://doi.org/10.3390/IJMS15033640.

(7) Gentile, P.; Chiono, V.; Carmagnola, I.; Hatton, P. V. An Overview of Poly(Lactic-Co-

Glycolic) Acid (PLGA)-Based Biomaterials for Bone Tissue Engineering. *International Journal of Molecular Sciences*. Multidisciplinary Digital Publishing Institute February 2014, pp 3640–3659. https://doi.org/10.3390/ijms15033640.

(8) Nair, L. S.; Laurencin, C. T. Biodegradable Polymers as Biomaterials. *Progress in Polymer Science (Oxford)*. Pergamon August 2007, pp 762–798. https://doi.org/10.1016/j.progpolymsci.2007.05.017.

(9) Filipowska, J.; Pawlik, J.; Cholewa-Kowalska, K.; Tylko, G.; Pamula, E.; Niedzwiedzki, L.; Szuta, M.; Laczka, M.; Osyczka, A. M. Incorporation of Sol–Gel Bioactive Glass into PLGA Improves Mechanical Properties and Bioactivity of Composite Scaffolds and Results in Their Osteoinductive Properties. *Biomed. Mater.* **2014**, *9* (6), 65001. https://doi.org/10.1088/1748-6041/9/6/065001.

(10) Mo, Y.; Guo, R.; Liu, J.; Lan, Y.; Zhang, Y.; Xue, W.; Zhang, Y. Preparation and Properties of PLGA Nanofiber Membranes Reinforced with Cellulose Nanocrystals. *Colloids Surfaces B Biointerfaces* **2015**, *132*, 177–184. https://doi.org/10.1016/J.COLSURFB.2015.05.029.

(11) Rasoulianboroujeni, M.; Fahimipour, F.; Shah, P.; Khoshroo, K.; Tahriri, M.; Eslami, H.; Yadegari, A.; Dashtimoghadam, E.; Tayebi, L. Development of 3D-Printed PLGA/TiO2 Nanocomposite Scaffolds for Bone Tissue Engineering Applications. *Mater. Sci. Eng. C* **2019**, *96*, 105–113. https://doi.org/10.1016/J.MSEC.2018.10.077.

(12) Wei, J.; Yan, Y.; Gao, J.; Li, Y.; Wang, R.; Wang, J.; Zou, Q.; Zuo, Y.; Zhu, M.; Li, J. 3D-Printed Hydroxyapatite Microspheres Reinforced PLGA Scaffolds for Bone Regeneration. *Biomater. Adv.* **2022**, *133*, 112618. https://doi.org/10.1016/J.MSEC.2021.112618.

(13) Qi, Z.; Guo, W.; Zheng, S.; Fu, C.; Ma, Y.; Pan, S.; Liu, Q.; Yang, X. Enhancement of Neural Stem Cell Survival, Proliferation and Differentiation by IGF-1 Delivery in Graphene Oxide-Incorporated PLGA Electrospun Nanofibrous Mats. *RSC Adv.* **2019**, *9* (15), 8315–8325. https://doi.org/10.1039/C8RA10103E.

(14) Dastagir, K.; Dastagir, N.; Limbourg, A.; Reimers, K.; Strauß, S.; Vogt, P. M. In Vitro Construction of Artificial Blood Vessels Using Spider Silk as a Supporting Matrix. *J. Mech. Behav. Biomed. Mater.* **2020**, *101* (August 2019), 103436. https://doi.org/10.1016/j.jmbbm.2019.103436.

(15) Cheng, S. W.; Widyananta, B. J.; Priosoeryanto, B. P. PF-35 Spider Silk (Nephilia Sp.) as Suture Material on Blood Vessel Surgery. In *Proc. of the 20th FAVA CONGRESS & The 15th IVMA KIVNAS PDHI, Bali*; 2018; p 585.

(16) Petzold, J.; Aigner, T. B.; Touska, F.; Zimmermann, K.; Scheibel, T.; Engel, F. B. Surface Features of Recombinant Spider Silk Protein EADF4(K16)-Made Materials Are Well-Suited for Cardiac Tissue Engineering. *Adv. Funct. Mater.* **2017**, *27* (36), 1701427. https://doi.org/10.1002/ADFM.201701427.

(17) Rockwood, D. N.; Preda, R. C.; Yücel, T.; Wang, X.; Lovett, M. L.; Kaplan, D. L. Materials Fabrication from Bombyx Mori Silk Fibroin. *Nat. Protoc. 2011 610* **2011**, *6* (10), 1612–1631. https://doi.org/10.1038/nprot.2011.379.

(18) Bobylev, D.; Wilhelmi, M.; Lau, S.; Klingenberg, M.; Mlinaric, M.; Petená, E.; Helms, F.; Hassel, T.; Haverich, A.; Horke, A.; Böer, U. Pressure-Compacted and Spider Silk–Reinforced Fibrin Demonstrates Sufficient Biomechanical Stability as Cardiac Patch in Vitro. *J. Biomater. Appl.* **2022**, *36* (6), 1126–1136.

https://doi.org/10.1177/08853282211046800.

(19) Scheibel, T. Spider Silks: Recombinant Synthesis, Assembly, Spinning, and Engineering of Synthetic Proteins. *Microb. Cell Fact.* **2004**, *3*, 1–10. https://doi.org/10.1186/1475-2859-3-14.

(20) Qin, D.; Wang, M.; Cheng, W.; Chen, J.; Wang, F.; Sun, J.; Ma, C.; Zhang, Y.; Zhang, H.; Li, H.; Liu, K.; Li, J. Spidroin-Mimetic Engineered Protein Fibers with High Toughness and Minimized Batch-to-Batch Variations through β-Sheets Co-Assembly. *Angew. Chemie Int. Ed.* **2024**, *63* (15), e202400595. https://doi.org/10.1002/ANIE.202400595.

(21) Gomes, V.; Salgueiro, S. P. From Small to Large-Scale: A Review of Recombinant Spider Silk and Collagen Bioproduction. *Discov. Mater.* **2022**, *2* (1), 3. https://doi.org/10.1007/s43939-022-00024-4.

(22) Huemmerich, D.; Scheibel, T.; Vollrath, F.; Cohen, S.; Gat, U.; Ittah, S. Novel Assembly Properties of Recombinant Spider Dragline Silk Proteins. *Curr. Biol.* **2004**, *14*, 2070–2074. https://doi.org/10.1016/j.cub.2004.11.005.

(23) Wohlrab, S.; Müller, S.; Schmidt, A.; Neubauer, S.; Kessler, H.; Leal-Egaña, A.; Scheibel, T. Cell Adhesion and Proliferation on RGD-Modified Recombinant Spider Silk Proteins. *Biomaterials* **2012**, *33* (28), 6650–6659. https://doi.org/10.1016/j.biomaterials.2012.05.069.

(24) ASTM F 756 - 00. Standard Practice for Assessment of Hemolytic Properties of Materials. ASTM International: West Conshohocken, PA, USA 2000. www.astm.org.

(25) Tiwari, S. K.; Venkatraman, S. S. Importance of Viscosity Parameters in Electrospinning: Of Monolithic and Core–Shell Fibers. *Mater. Sci. Eng. C* **2012**, *32* (5), 1037–1042. https://doi.org/10.1016/J.MSEC.2012.02.019.

(26) Zhou, S.; Peng, H.; Yu, X.; Zheng, X.; Cui, W.; Zhang, Z.; Li, X.; Wang, J.; Weng, J.; Jia, W.; Li, F. Preparation and Characterization of a Novel Electrospun Spider Silk Fibroin/Poly(D,L-Lactide) Composite Fiber. *J. Phys. Chem. B* **2008**, *112* (36), 11209–11216. https://doi.org/10.1021/jp800913k.

(27) Włoch, M.; Datta, J. Rheology of Polymer Blends. In *Rheology of Polymer Blends and Nanocomposites: Theory, Modelling and Applications*; Elsevier, 2019; pp 19–29. https://doi.org/10.1016/B978-0-12-816957-5.00002-1.

(28) Singh, G.; Kaur, T. K.; Kaur, R.; Kaur, A. Recent Biomedical Applications and Patents on Biodegradable Polymer-. *Int. J. Pharmacol.* **2014**, No. January, 30–42.

(29) Griffiths, P. R.; de Haseth, J. A. *Fourier Transform Infrared Spectrometry*; Wiley, 2007. https://doi.org/10.1002/047010631X.

(30) Silverstein, Robert M.; Webster, Franis X.; Kiemle, David J.; Bryce, D. *Spectrometric Identification of Organic Compounds*, 8th ed.; Wiley, 2014.

(31) Eren Boncu, T.; Ozdemir, N.; Uskudar Guclu, A. Electrospinning of Linezolid Loaded PLGA Nanofibers: Effect of Solvents on Its Spinnability, Drug Delivery, Mechanical Properties, and Antibacterial Activities. *Drug Dev. Ind. Pharm.* **2020**, *46* (1), 109–121. https://doi.org/10.1080/03639045.2019.1706550.

(32) Meng, Z. X.; Zheng, W.; Li, L.; Zheng, Y. F. Fabrication, Characterization and in Vitro Drug Release Behavior of Electrospun PLGA/Chitosan Nanofibrous Scaffold. *Mater. Chem. Phys.* **2011**, *125* (3), 606–611.

https://doi.org/10.1016/J.MATCHEMPHYS.2010.10.010.

(33) Sheik, S.; Karikannar Nagaraja, G. Development, Characterization and Properties of Silk Fibre and Grafted Silk Fibre Reinforced Polymer Composite Films. In *Generation, Development and Modifications of Natural Fibers*; IntechOpen, 2020. https://doi.org/10.5772/intechopen.85022.

(34) Venkatesan, H.; Hu, J.; Chen, J. Bioinspired Fabrication of Polyurethane/Regenerated Silk Fibroin Composite Fibres with Tubuliform Silk-Like Flat Stress–Strain Behaviour. *Polym. 2018, Vol. 10, Page 333* **2018**, *10* (3), 333. https://doi.org/10.3390/POLYM10030333.

(35) Gao, A.; Yang, Q.; Xue, L. Poly (l-Lactic Acid)/Silk Fibroin Composite Membranes with Improved Crystallinity and Thermal Stability from Non-Solvent Induced Phase Separation Processes Involving Hexafluoroisopropanol. *Compos. Sci. Technol.* **2016**, *132*, 38–46. https://doi.org/10.1016/j.compscitech.2016.06.011.

(36) Dobhal, A.; Srivastav, A.; Dandekar, P.; Jain, R. Influence of Lactide vs Glycolide Composition of Poly (Lactic-Co-Glycolic Acid) Polymers on Encapsulation of Hydrophobic Molecules: Molecular Dynamics and Formulation Studies. *J. Mater. Sci. Mater. Med.* **2021**, *32* (10), 1–18. https://doi.org/10.1007/s10856-021-06580-0.

(37) Qiao, X.; Li, W.; Sun, K.; Xu, S.; Chen, X. Isothermal Crystallization Kinetics of Silk Fibroin Fiber-Reinforced Poly(ε-Caprolactone) Biocomposites. *Polym. Int.* **2009**, *58* (5), 530–537. https://doi.org/10.1002/pi.2563.

(38) Lipson, J. E. G. Global and Local Views of the Glass Transition in Mixtures. *Macromolecules*. 2020, pp 7219–7223. https://doi.org/10.1021/acs.macromol.0c01455.

(39) Abiad, M. G.; Carvajal, M. T.; Campanella, O. H. A Review on Methods and Theories to Describe the Glass Transition Phenomenon: Applications in Food and Pharmaceutical Products. *Food Eng. Rev. 2009 12* **2009**, *1* (2), 105–132. https://doi.org/10.1007/S12393-009-9009-1.

(40) Li, W.; Olvera De La Cruz, M. Glass Transition of Ion-Containing Polymer Melts in Bulk and Thin Films. *Soft Matter* **2021**, *17* (37), 8420–8433. https://doi.org/10.1039/D1SM01098K.

(41) Xie, R.; Weisen, A. R.; Lee, Y.; Aplan, M. A.; Fenton, A. M.; Masucci, A. E.; Kempe, F.; Sommer, M.; Pester, C. W.; Colby, R. H.; Gomez, E. D. Glass Transition Temperature from the Chemical Structure of Conjugated Polymers. *Nat. Commun.* **2020**, *11* (1). https://doi.org/10.1038/s41467-020-14656-8.

(42) Khan, R. A. A.; Chen, X.; Qi, H. K.; Huang, J. H.; Luo, M. B. A Novel Shift in the Glass Transition Temperature of Polymer Nanocomposites: A Molecular Dynamics Simulation Study. *Phys. Chem. Chem. Phys.* **2021**, *23* (21), 12216–12225. https://doi.org/10.1039/d1cp00321f.

(43) Julbe, A.; Drobek, M. Glass Transition Temperature (T G ). *Encycl. Membr.* **2016**, 878–880. https://doi.org/10.1007/978-3-662-44324-8_267.

(44) Kramer, J. P. M.; Aigner, tamara B.; Petzold, J.; Roshanbinfar, K.; Scheibel, T.; Engel, felix B. Recombinant Spider Silk Protein EADF4(C16)-RGD Coatings Are Suitable for Cardiac Tissue Engineering. *Sci. Rep.* **2020**, *10* (1). https://doi.org/10.1038/s41598-020-65786-4.

(45) Kramer, J. P. M.; Aigner, T. B.; Petzold, J.; Roshanbinfar, K.; Scheibel, T.; Engel, F. B.

Recombinant Spider Silk Protein EADF4(C16)-RGD Coatings Are Suitable for Cardiac Tissue Engineering. *Sci. Rep.* **2020**, *10* (1), 8789–8789. https://doi.org/10.1038/s41598-020-65786-4.

(46) Lang, G.; Grill, C.; Scheibel, T. Site-Specific Functionalization of Recombinant Spider Silk Janus Fibers. *Angew. Chemie - Int. Ed.* **2022**, *61* (11). https://doi.org/10.1002/ANIE.202115232.